Rare Metal Materials and Engineering
Volume 47, Issue 1, January 2018
Online English edition of the Chinese language journal

Available online at www.sciencedirect.com
ScienceDirect

Cite this article as: Rare Metal Materials and Engineering, 2018, 47(1): 0020-0025.

ARTICLE

Effect of Ultra-fine WC Particles on Microstructural Evolution and Wear Behavior of Ni-Based Nano-CeO_2 Coatings Produced by Laser

Zhao Ning[1,2], Tao Li[1,2], Guo Hui[1,2], Zhang Mengqi[1,2]

[1] Northwestern Polytechnical University, Xi'an 710072, China; [2] Shaanxi Engineering Laboratory for Transmissions and Controls, Xi'an 710072, China

Abstract: The wear behavior and microstructure of CO_2 laser cladded Ni-based alloy coatings with 1 wt% nano-CeO_2 and 20 wt% WC addition (CeO_2/Ni) was compared with Ni-based coatings with 1 wt% nano-CeO_2 addition (WC-CeO_2/Ni). Both coatings were cladded on 30CrMnSiNi2A steel with good metallurgical bounding to substrate. The influence of ultra-fine carbide WC on the microstructure of WC-CeO_2/Ni alloy composite coatings were investigated by X-ray diffraction (XRD), scanning electron microscopy (SEM) coupled with energy dispersive spectroscopy (EDS) and electron probe micro analysis (EPMA). WC addition increased $M_{23}C_6$ content, but decreased the M_7C_3. The comparison of comprehensive mechanical properties between coatings with and without fine WC particles was conducted on Vickers hardness and wear-resistance test system. Results indicate that the performance of WC-CeO_2/Ni is better than that of CeO_2/Ni metal matrix composition (MMC). Few hot cracks appeared in Ni-based WC-CeO_2 MMC production, which were investigated by SEM and EDS. The crack mechanism can be claimed as Fe dilution and coefficient of thermal expansion for WC-CeO_2/Ni MMC differed from that of base material 30CrMnSiNi2A steel.

Key words: Ce; tribo-mechanical properties; laser; Ni-based alloy; WC

The practical application of laser cladding wear resistance overlays on steel work piece surface could endure particularly aggressive conditions which embrace severely abrasive wear, heavy load and erosion wear resistance. The lifespan of machine can be increased by hard facing surface treatments and/or coatings [1]. The laser cladded layers, especially Ni-based alloy metal matrix composites (MMC), have attracted extensive attention for their excellent comprehensive mechanical properties including wear resistance, Vickers hardness, corrosion resistance, toughness as well as production efficient and reliable metallurgical bounding to the substrate. Among many available hard reinforcement particles in Ni-based alloy, WC possessed favorable wettability with matrix Ni (and some Fe from base steel) and the existence of transition bounding layer between WC and bounding metal demonstrated the particles were perfectly imbedded in MMC. The macro-mechanical of MMC materials related to thermo physical properties of Ni-based alloy, hard particles and even substrate materials convection currents in the melt pool during the solidification procedure. Both the WC and W_2C hard phases improved the hardness of Ni-based MMC. RE and RE oxidation can refine laser coating microstructure and increase micro-hardness. La and Ce improved AM60 abrasion and corrosive properties according to Liang Chenghao et al[2].

The dissolution of WC in laser melt pool was mentioned in the paper published by S. Zhou et al. [3] in which $M_{23}C_6$ and M_7C_3 were also as precipitated carbides. The reinforcement $M_{23}C_6$ combined with γ-Ni(Fe) matrix were reported in the research of T. Yu et al. [4] The decrease of coarse carbide and eutectic in MMC improve the coating quality, reducing the crack susceptibility.

The cracks generated in and after laser layer production are

Received date: January 14, 2017
Foundation item: National Natural Science Foundation of China (51075328, 51675424); Fundamental Research Funds for the Central Universities (3102015BJ (II) MYZ28)
Corresponding author: Zhao Ning, Ph. D., Professor, School of Mechatronics, Northwestern Polytechnical University, Xi'an 710072, P. R. China, Tel: 0086-29-88460507, E-mail: npuzhaon@163.com

Copyright © 2018, Northwest Institute for Nonferrous Metal Research. Published by Elsevier BV. All rights reserved.

hot cracks and cold cracks due to latent heat, high thermal stress, structural stress and low yield strength. The high thermal stress and large temperature gradient in narrow laser tracks brought by high speed laser scanning caused crack sensitivity increment, while residual stress formed the potential driven force for crack development[5]. An inappropriate high volume fraction of WC_p in MMC also contributed to cracks formation. This can be understood by the fact that dense WC_p content could form eutectic phases γ+carbides which paved the way for cracks propagation[6]. Hot crack 3D simulation was developed in the study of Chao Yanpu et al[7].

1 Experiment

1.1 Powders and substrate metal

Ultra-fine single crystal WC particles, nanometer CeO_2 and spherical Ni-based alloy powders were used in this research. The average particle size of WC was 2 μm and size range was from 0.5 to 2.5 μm. Both of the 2 μm WC and 40 nm CeO_2 were of 99.99% purity. The mean diameter for Ni-based alloy spherical particles was 60 μm. The compositions of base material and Ni-based alloy are shown in Table 1. The mentioned materials were fully blended in a mechanical grinding machine at 600 r/min for 12 h. The mixing ratio are shown in Table 2.

Ultra-high-strength steel 30CrMnSiNi2A was selected as substrates and cut to the size of 12 mm×60 mm×140 mm. The substrate metal was ground by sandpapers from 37 μm to 10 μm to get rid of surface oxidation and then bathed in ultrasonic acetone for 30 min for degreasing. Prior to laser cladding, the blended powders and substrate metal were dried in vacuum stove at 150 °C for 2 h.

1.2 Laser cladding

The wear-resistant coatings were laser cladded by a 5 kW Convergent CP4000 CO_2 laser system. Nitrogen was chosen as laser processing atmosphere in air pressure of 0.55 MPa in the chamber to eliminate oxidation. Laser beam was fixed to a diameter of 2 mm and the diameter of melt pool was around 3 mm; length of each straight line laser scanning trace was 45 mm; laser scanning speed was 8 mm/s; single directional scanning; single layer cladding; laser tracks overlapping rate was 25%; preplaced powder bed thickness was 3 mm; as-cladded layer thickness 0.5 mm to 1 mm. Details as shown in Fig.1.

Table 1 Chemical composition of 30CrMnSiNi2A and Ni-based alloy (wt%)

Element	30CrMnSiNi2A	Ni-based alloy
C	0.27~0.34	0.5
Mn	1.00~1.30	-
Cr	0.90~1.20	20.0
Si	1.20	3.5
Ni	1.40~1.80	Bal.
S	≤0.015	-
P	≤0.025	-
Fe	Bal.	≤5.0
B	-	3.0

Table 2 Coatings prepared with different feedstock fractions (mass fraction)

Coatings	Cladding materials
Ce/Ni	1%CeO_2-99%Ni-based alloy
WC-Ce/Ni	20%WC-1%CeO_2-79%Ni-based alloy

1.3 Sample observation

The cladded specimens were ground by wheel and sandpaper from 37 μm to 4 μm then polished for XRD or further etched for SEM and EPMA observation.

Fig.2 shows the different XRD patterns of Ce/Ni and WC-Ce/Ni MMC coatings. WC phase was not detected in both XRD pattern, which reflects a low content level of WC crystallization. The crystallization of W_2C is also too low to be discovered. Both WC and W_2C exist but their content are too low to be detected. The WC decomposition may be caused by the high energy laser radiation, WC suffered from severe heat concentration and interacted with Ni-based alloy matrix rich in Fe and Cr.[3] Considering the 20 wt% WC particles content in blended powder, this phenomena can be interpreted by the further decomposition of dissolved W_2C into W and C in which the C atom involved in $Cr_{23}C_6$ and Cr_7C_3 formation while metal W either mixed with eutectic+carbides or formed $(Cr,W)_{23}C_6$. The transition mechanism of metastable phase M_7C_3 into $M_{23}C_6$ can be described in Formula (1) where the letter M represents metal Cr and W. Formula (2) illustrates the C atom from M_7C_3 reacted with the element Cr in metal

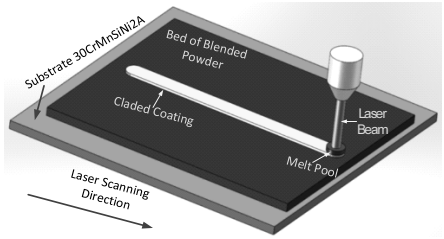

Fig. 1 Diagrammatic sketch of laser processing

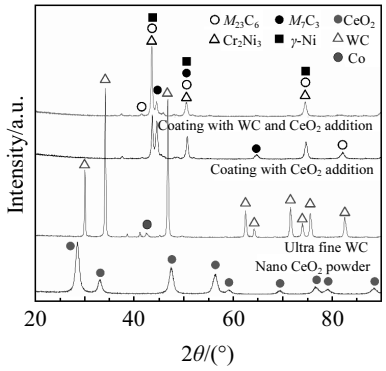

Fig. 2 XRD patterns of laser cladding Ce/Ni and WC-Ce/Ni coatings

matrix and thus more $Cr_{23}C_6$ formed.[8] The γ-Ni(Fe) solid solu tion whose characteristic peaks 2θ of 43.5°, 50.6° and 74.5° are definitely the predominating matrix phase for both coatings. Compared with the XRD pattern of Ce/Ni coating in red colour, the obvious intensity increment of peak γ-Ni(Fe), $M_{23}C_6$ and Cr_3Ni_2 phase located 43.5° in black WC-Ce/Ni pattern probably reflect the increased amount of $M_{23}C_6$ in WC-Ce/Ni MMC. The γ-Ni(Fe) in WC-Ce/Ni MMC companioned with few residual WC and newly formed W_2C, chrome-rich phase $Cr_{23}C_6$, Cr_7C_3 and Cr_2Ni_3 as well as Cr_3Ni_2. The absence of diffraction peaks belonging to the Cr_7C_3 located about 46° is the evidence for low amount and/or low Cr_7C_3 crystallinity in WC-Ce/Ni MMC coating.

$$23M_7C_3 \rightarrow 7M_{23}C_6 + 27C \quad (1)$$

$$6C + 23Cr \rightarrow Cr_{23}C_6 \quad (2)$$

2 Results and Discussion

2.1 Surface analyses and hardness

The cross-sectional microstructure of Ce/Ni and WC-Ce/Ni laser coatings are shown in Fig.3.

The micro morphology of WC-CeO_2/Ni coating in Fig. 3b is more homogeneously than CeO_2/Ni coating in Fig. 3a. The presence of fine, feather-like secondary phase in Fig. 3d can be specifically associated to the precipitate either partially or fully melted WC eutectic carbide in WC-CeO_2/Ni coating. From Fig.3c~3h, a conclusion can be reached that the WC-CeO_2/Ni coating possesses thicker eutectic film and less secondary dendrite distance than CeO_2/Ni coating.

Statistically, the percentage of eutectic and carbides in Fig. 3c, 3d, 3e, 3f, 3g, 3h are 49.03%, 70.35%, 45.18%, 47.90%, 38.33% and 42.25%, respectively. It is obvious the WC addition dissolved in WC-Ce/Ni MMC apparently increases carbide amount in eutectic and thus decreases the second dendrite inter space, seen in Fig.3d, 3f.

The hardness of different coatings also reflects the effect of hardness improvement of fine WC particles addition on MMC. The Vickers hardness $HV_{0.5}$ of WC-Ce/Ni coating varied from about 8200 MPa to 10200 MPa in Fig. 4b. The Ce/Ni coating displays a much lower hardness value which fluctuates around 4600 MPa in Fig.4a. This improvement in hardness of WC-Ce/Ni coating can be explained by the W and C atom from WC particles dissolved into binder metal: (i) C atom mainly from WC addition facilitates the formation of hard and brittle phase carbide e.g. $M_{23}C_6$; (ii) solid solution hardening, dissolved W as solid solution element improves lattice distortion[3].

2.2 Wear property and coating microstructure

The microstructure results in Fig.3 are combined with wear property which are displayed in Fig.5. The partially dissolved WC in feather-like eutectic improves coating microhardness and wear property. Less secondary dendrite space of WC-Ce/Ni layer seen in Fig. 3d, 3f also contributes to dense microstructure and better comprehensive mechanical performance. Meantime, the Ce in Ni-Ce coating segregated in interdendrite eutectic is shown in Fig.6. The Ce refines the microstructure and enhances abrasive resistance in turn. Fig.5 shows the wear volume loss rate of the coating samples and base steel at the speed of 8 mm/s at load 25 N, room temperature.

The wear volume loss rate for three coating samples and substrate metal are shown in Fig.5. The coating specimen with CeO_2 and ceramic particle WC addition displays the best wear resistance with wear volume loss rate 1.36 $mm^3/N \cdot m$, followed by the nickel alloy with 1 wt% CeO_2 addition whose wear volume loss rate is 2.14 $mm^3/N \cdot m$. Both pure nickel alloy and 30CrMnSiNi2A substrate show comparatively low abrasive resistance and their wear volume loss rate values are 4.20 and 11.55 $mm^3/N \cdot m$, respectively.

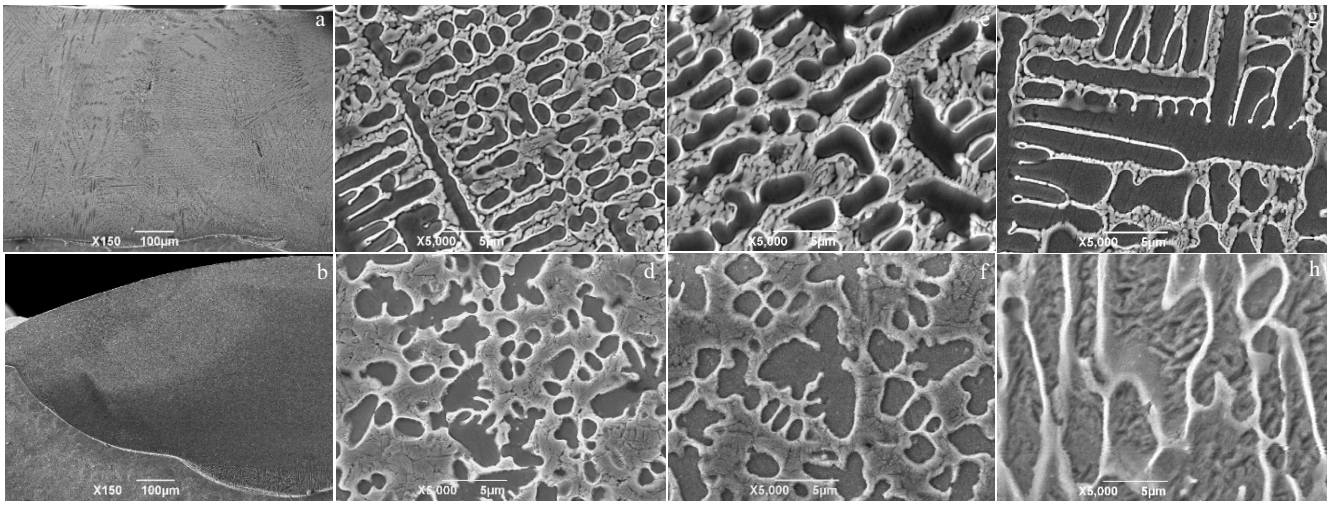

Fig. 3 SEM morphologies of CeO_2/Ni coating (a, c, e, g) and WC-CeO_2 coating (b, d, f, h): (a, b) overall morphology, (c, d) top region, (e, f) middle region, and (g, h) bottom region

2.3 Explanation of cracks

Fig.7 shows the SEM micrograph of coating hot crack cross section, and it is clear that the microstructure of coating in the left side of crack is uniform and compact without any macro cracks nor pores. Different phases in fracture region in the composite layers can be analyzed by EDS point scanning in Fig.7. Fine hard particles of different morphology are embedded in matrix metal. Angular particles are pulled out along the crack surface as can be seen in the two ellipse regions marked No.1 and No.2 in Fig.7a. This indicates the existence of intergranular fracture. The detailed phases EDS results are presented in Table 3. According to Table 3, the atom ratio in area A in Fig.5b is Ce:O≈1:2 and area B is mainly Fe and Ni; therefore the microstructure of area A can be recognized as CeO_2 and phase B as the γ-(Fe, Ni). The CeO_2 in Fig.6b is mostly distributed in inter-dendrite.

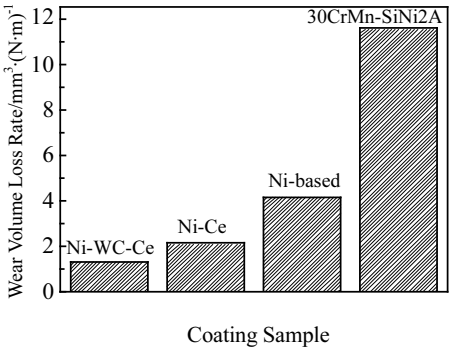

Fig.5 Wear volume loss rate of the coating samples dry sliding at 25 N

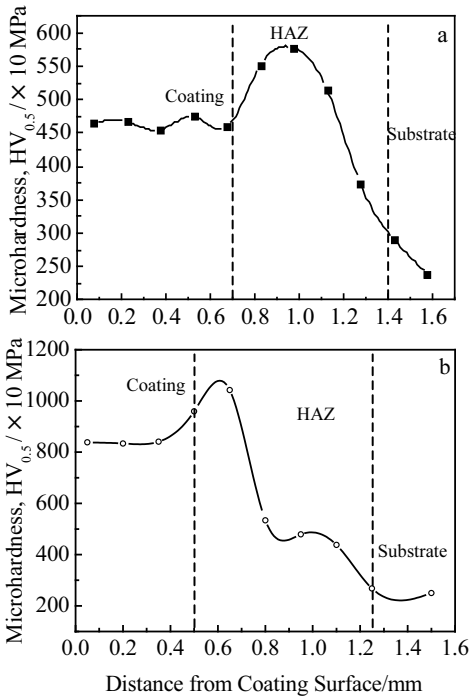

Fig.4 Vickers hardness of Ce/Ni (a) and WC-Ce/Ni (b) coating

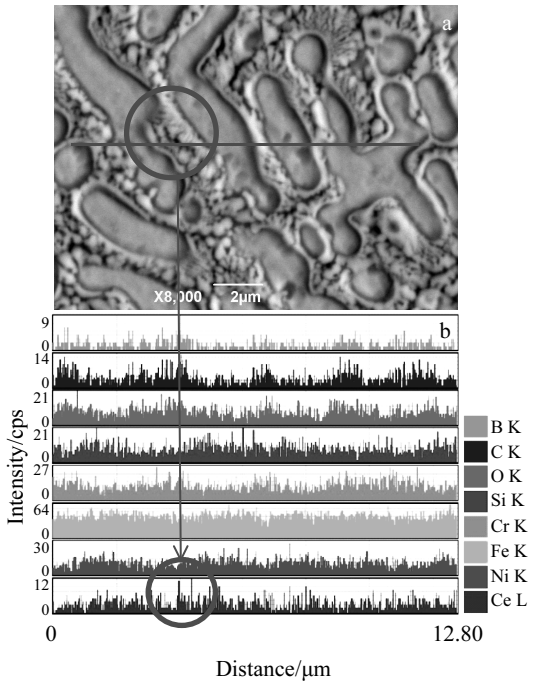

Fig.6 SEM image and Ce distribution along interdentrite of Ce/Ni MMC

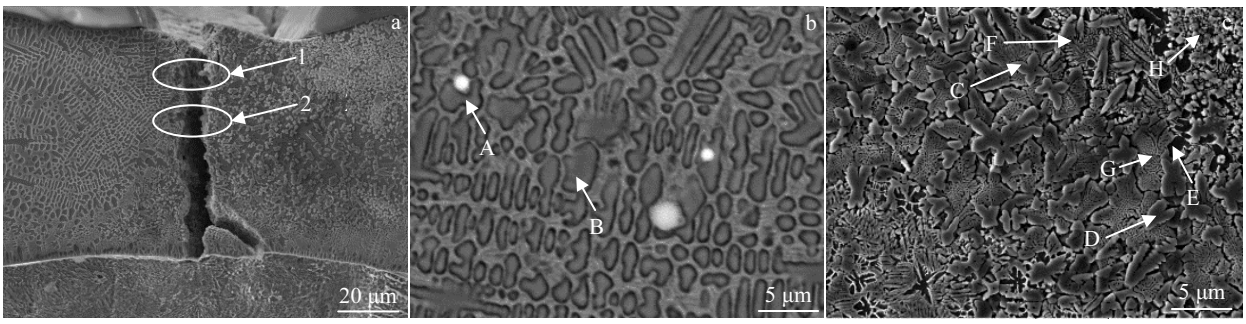

Fig.7 SEM morphologies of crack cross-section: (a) overall, (b) typical microstructure of left side of the crack, (c) typical microstructure of right side of the crack

Table 3 Elemental distribution of regions marked in Fig.7b, and 7c (at%)

Region	C	B	Si	Cr	Fe	Ni	W	Ce	Mn	O
A	-	-	-	-	18.58	4.19	1.49	28.33	-	47.41
B	-	-	3.55	5.52	66.99	20.95	2.16	-	0.83	-
C	-	-	-	26.24	20.86	31.85	21.05	-	-	-
D	-	57.00	2.14	8.51	6.12	10.48	15.76	-	-	-
E	-	-	9.33	5.43	26.66	58.58	-	-	-	-
F	22.82	-	-	6.68	30.16	37.78	2.56	-	-	-
G	4.87	-	-	9.84	38.84	44.47	1.98	-	-	-
H	32.03	-	-	11.27	9.97	24.29	22.43	-	-	-

The major element in the crisscross-like pattern phase C is nickel together with some tungsten, chrome and iron. Based on the EDS result, the morphological feature phase C can be identified as typical inner precipitated phase which is formed by partially melting on the original WC particles surface and dissociative tungsten atoms distributed in the Ni-based alloy matrix (Fig.7c). The atom fraction of boron in the block precipitate phase D is more than 50%, together with some W, Ni, Cr and Fe.

The small dark grey polygonal phase marked E in Fig.7c contains a high concentration of nickel and some iron. The carbon-rich region of network area phase F and G possesses the atom ratio of carbon:metal≈3:7 and carbon:metal≈6:23 which can be reckoned as M_7C_3 and $M_{23}C_6$ according to XRD result, respectively.

The difference of linear expansion coefficients between Ni-based alloy and the precipitated hard phase material causes local residual stress concentration along crack propagation surface. The absorption of latent heat increases ceramic phase volume during liquid-solid transformation cycle. The left side of crack cross-section displays smaller expansion coefficient. The residual stress in coating generated during cooling after laser processing is larger than yield strength. In conclusion, the clusters of hard phase particles form crack initiation sites for brittle cold cracks.

To explain the mechanism of hot crack forming, Fig.8 shows EPMA line scan of Fe dilution from laser melt pool to coating surface is crucial.

As mentioned before, the area percentage of eutectic and carbides in Fig.3f, 3g are 15.67% and 19.18%, respectively. It is clear that there is more eutectic and carbides in WC-Ce/Ni than Ce/Ni MMC. Increased eutectic content combined with widened solidification temperature range (STR) induces a higher crack sensibility.

Fig.9 shows the different linear expansion coefficent of three coatings. It is apparent that from 700 °C to 0 °C the linear expansion coefficient of WC-Ce/Ni drops far below those of Ce/Ni and base metal 30CrMnSiNi2A. The three curves in Fig.9 clearly explain the phenomena of well-matched Ce/Ni MMC and base metal and no-match WC-Ce/Ni and base metal in the solidification procedure below 700 °C.

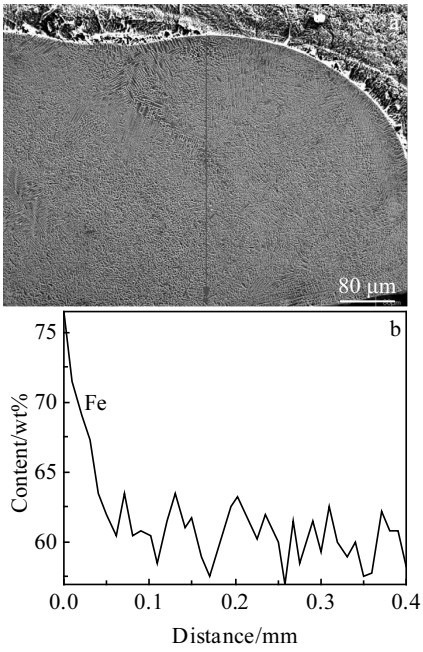

Fig.8 EPMA line scan position (a) and Fe distribution along depth (b) of WC-Ce/Ni MMC

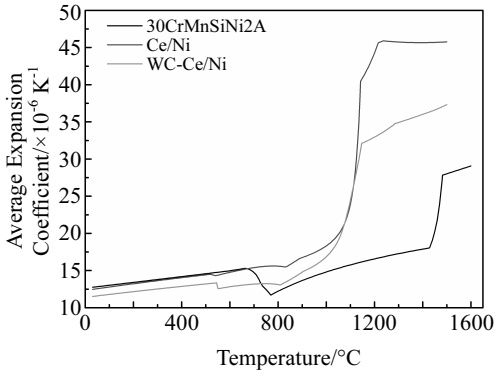

Fig.9 Coefficient of linear thermal expansion for different MMCs

3 Conclusions

1) The Ni-based CeO_2 and WC-CeO_2 MMC coatings are metallurgically well bounded to 30CrMnSiNi2A with a strong coating/substrate fusion interface. The nano-CeO_2 concentrated in inter-dendrite eutectic, therefore, restricts the grain size and thus promotes fine microstructure formation in CeO_2/Ni and WC-CeO_2/Ni MMC.

2) The addition of WC is partially dissolved and C atom accelerates $M_{23}C_6$ formation. The amount of M_7C_3 decreases in WC-CeO_2/Ni MMC. Additionally, the Vickers hardness and wear volume loss rate of Ni-based WC-CeO_2 MMC coatings are better than those of the Ni-based CeO_2 MMC coatings.

3) A few cracks appear only in the fringe of multi-tracks WC-CeO_2/Ni MMC coatings and mainly propagate parallel to laser scanning direction and can be identified as hot cracks. There is ununiform Fe distribution along WC-CeO_2/Ni MMC depth; therefore solidification temperature range differs between coating bottom and surface. The dissolved WC reduces coefficient of thermal linear expansion which also contribute to hot crack generation. No crack appears in Ni-based CeO_2 coatings. Both coatings have no pores.

References

1 Zikin A Badisch, E, Hussainova, I *et al. Surface & Coatings Technology*[J], 2013, 236: 36

2 Liang Chenghao, Wang Shusen, Huang Naibo *et al. Rare Metal Materials and Engineering*[J], 2015, 44(3): 521

3 Zhou Shengfeng, Lei Jianbo, Dai Xiaoqin *et al. Int Journal of Refractory Metals and Hard Metals*[J], 2016, 60: 17

4 Yu Ting, Deng Qilin, Dong Gang *et al. Applied Surface Science*[J], 2011, 257: 5098

5 Lee C, Park, Yoo J *et al. Appl Surf Sci*[J], 2015, 345: 286

6 Wang Jiandong, Li Liqun, Tao Wang. *Optics & Laser Technology*[J], 2016, 82: 170

7 Chao Yanpu, Qi Lehua, Bai Zhengmin. *Rare Metal Materials and Engineering*[J], 2016, 45(8): 1924

8 Guo Jianting. *Materials Science and Engineering for Superalloys* [M]. Beijing: Science Press, 2010: 299 (in Chinese)

超细 WC 颗粒对纳米 CeO_2 增强激光镍基涂层的显微组织和耐磨性影响

赵　宁[1,2]，陶　礼[1,2]，郭　辉[1,2]，张蒙祺[1,2]

(1. 西北工业大学，陕西 西安 710072)

(2. 陕西省机电传动与控制工程实验室，陕西 西安 710072)

摘　要：CO_2 激光器熔覆质量分数 1%纳米 CeO_2 和 20%WC 添加的镍基合金涂层的磨损、显微组织与 1%纳米 CeO_2 添加镍基合金涂层进行对比。上述 2 种涂层均熔覆在基体 30CrMnSiNi2A 上并呈优良冶金结合。超细碳化物 WC 对 WC-CeO_2/Ni 涂层的显微组织影响由 X 射线衍射（XRD），扫描电镜（SEM）连同能谱（EDS），电子探针（EPMA）进行分析。添加 WC 后 $M_{23}C_6$ 增多，而 M_7C_3 减少。通过维氏硬度计和磨损测试系统对有 WC 添加和未添加 CeO_2 镍基合金涂层进行综合机械性能比。得出 WC-CeO_2/Ni 涂层明显优于 CeO_2/Ni 涂层。极少数热裂纹出现于 WC-CeO_2/Ni 涂层，萌生并扩展于熔池凝固过程中，对此做了 SEM 和 EDS 分析。裂纹机理可归因为铁稀释和 WC 添加导致的涂层与基体 30CrMnSiNi2A 间线膨胀系数间差异。

关键词：Ce；机械磨损性能；激光；镍基合金；WC

作者简介：赵　宁，男，1958 年生，博士，教授，西北工业大学机电学院，陕西 西安 710016，电话：029-88460507，E-mail: npuzhaon@163.com